Journal of Materials Chemistry

PAPER

Electrically controlled electron transfer and resistance switching in reduced graphene oxide noncovalently functionalized with thionine

Benlin Hu,[a] Ruge Quhe,[b] Cao Chen,[c] Fei Zhuge,[a] Xiaojian Zhu,[a] Shanshan Peng,[a] Xinxin Chen,[a] Liang Pan,[a] Yuanzhao Wu,[a] Wenge Zheng,[c] Qing Yan,[a] Jing Lu[b] and Run–Wei Li[*a]

We demonstrate the electrically controlled electron transfer of thionine-functionalized reduced graphene oxide (rGO–th) in the form of a homogeneous solution and films. The electron transfer can be realized in a bidirectional way, which provides a method to control the electronic properties of graphene through π–π noncovalent functionalization. Based on the aforementioned controllable electron transfer between graphene sheets and thionine, resistance random access memories with a configuration of Pt/rGO–th/Pt were fabricated and show nonvolatile resistive switching with a large ON/OFF ratio of more than 10^4, fast switching speed of <5 ns, long retention time of over 10^5 s and excellent endurance. Furthermore, the reverse electron transfer between thionine and rGO as well as the resistive switching mechanism of the Pt/rGO–th/Pt devices were confirmed by density functional theory (DFT) calculation.

Introduction

Since its discovery in 2004,[1] graphene has attracted significant attention from both academic and commercial communities due to its unique structure, a monolayer of sp^2-hybridized carbon atoms tightly arranged into a two-dimensional honeycomb network.[2] This monolayer carbon material exhibits extraordinary thermal, mechanical and electrical properties, and has been applied in a variety of devices such as transistors,[3] solar cells,[4] lithium batteries[5] and memories.[6] As one of the most promising novel electronic and optoelectronic materials, controlling electron transfer in graphene-based hybrid systems becomes a critical issue, especially for device applications.[7] Recently, electron transfer between graphene sheets and dye molecules has been achieved by means of optical excitation.[7d,8] However, such electron transfer can only occur in a unidirectional way, *i.e.*, from dye molecules to graphene sheets. This unidirectional electron transfer restricts some potential applications, for example, writable/erasable memories. Therefore, to develop the potential of such a promising material in writable/erasable memories, it is necessary to achieve bidirectional or reversible electron transfer.

Resistive random access memories (RRAM) based on graphene oxide (GO) and its covalently functionalized derivatives have been reported.[6] The resistive switching mechanism has been explained by the electron transfer between GO and organic molecules or metal nanoparticles though there is no strong experimental evidence so far. Covalent functionalization is apt to destroy the electronic structure of graphene and involves toxic reagents as well as severe reaction conditions. However, noncovalent functionalization is viewed as a simple but effective way to obtain or modify graphene functionalities, which is friendly to the environment.[9] Herein, we report experimentally and theoretically on the electrically controlled reversible electron transfer between reduced graphene oxide (rGO) sheets and noncovalently bonded thionine (th) molecules. The thionine molecule (Scheme 1) has two hydrophilic amino-groups symmetrically distributed on each side and a planar aromatic structure that allows strong interaction with the surfaces of graphene sheets through synergistic noncovalent charge transfer and π–π stacking forces.[10] As expected, a layer-by-layer film is obtained by filtering the rGO–th solution and then transferring the rGO–th flakes to a substrate, and the Pt/rGO–th/Pt memory devices exhibit typical bistable electrical switching behavior and a nonvolatile rewritable memory effect, with a large ON/OFF resistance ratio, excellent endurance, fast switching speed and

[a]Key Laboratory of Magnetic Materials and Devices and Zhejiang Province Key Laboratory of Magnetic Materials and Application Technology, Ningbo Institute of Material Technology and Engineering, Chinese Academy of Sciences, Ningbo 315201, China. E-mail: runweili@nimte.ac.cn

[b]State Key Laboratory for Mesoscopic Physics and Department of Physics, Academy for Advanced Interdisciplinary Studies, Peking University, Beijing 100871, People's Republic of China

[c]Ningbo Key Laboratory of Polymer Materials, Ningbo Institute of Material Technology and Engineering, Chinese Academy of Sciences, Ningbo 315201, China
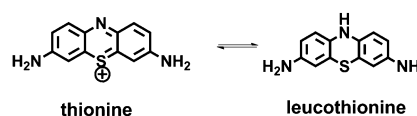
Scheme 1 The redox reaction between thionine and leucothionine.

long retention time. These results provide a new strategy for modulating the electric properties of graphene by a noncovalent modification with redox molecules with a large π electron system and also for fabricating resistive switching memory devices based on the electron transfer between graphene and functionalized molecules.

Experimental section

Characterization

High resolution transmission electron microscopy (HRTEM) studies were performed on a Tecnai F20 microscope. X-ray photoelectron spectroscopy (XPS) analysis was carried out on a Kratos AXIS ULTRA Multifunctional X-ray Photoelectron Spectroscope using Al (mono) K_α radiation (1488.6 eV). UV-vis absorption spectra were obtained using a PerkinElmer UV WinLab spectrophotometer. Fluorescence spectra were collected by a Hitach-F4600 fluorescence spectrometer. Cyclic voltammetric (CV) measurements were carried out with a CHI 832b Electrochemical Workstation (CH Instruments, Shanghai Chenhua Instrument Corporation, China). A three-compartment electrochemical cell contained a platinum wire auxiliary electrode, a saturated calomel reference electrode (SCE) and a bare or modified glassy carbon electrode (GCE, $\Phi = 2$ mm) was used as a working electrode. The GCE was polished with 1.0 μm, 0.3 μm, and 0.05 μm α-alumina powders and rinsed thoroughly with deionized water between each polishing step and sequentially sonicated in 1 : 1 HNO_3, ethanol, and deionized water, and dried at room temperature. A suspension of rGO–th (0.1 mg mL^{-1}) was coated on the GC electrode and dried at room temperature to obtain the rGO–th-modified GC electrode. Similarly, th-, rGO- and th/rGO- modified GC electrodes were prepared. The I–V characteristics were measured at room temperature by a Keithley 4200 semiconductor characterization system in voltage sweeping mode. During the measurement, a bias voltage was applied between the top and bottom (Pt) electrodes with the latter being grounded, unless otherwise specified.

Synthesis of GO and rGO–th

GO samples were prepared based on the modified Staudemire procedure.[11] rGO–th was synthesized through the reduction of GO in the presence of thionine. The GO aqueous solution (100 mL, 0.05 mg mL^{-1}) was heated to 40 °C by using a backflow device with vigorous stirring, then thionine (30 mg) was added into the solution. Once the temperature reached 90 °C, the mixture was reduced by hydrazine solution (8 μL, 35 wt% in water) for 12 h. After repeated centrifugation and washing with de-ionized water, the as-synthesized rGO–th was dispersed in water to give a 0.05 mg mL^{-1} dispersion.

Fabrication method of memory devices

rGO–th thin films of about 40 nm in thickness were prepared at room temperature by the vacuum filtration method. 50 mL of rGO–th suspension with a concentration of 6 mg L^{-1} was filtered through a cellulose ester membrane to achieve uniform rGO–th thin films. The film thickness could be well controlled by tuning the rGO–th concentration or filtration volume. The as-filtered

rGO–th flakes were then transferred from the filter membrane onto pre-cleaned commercial Pt/Ti/SiO$_2$/Si substrates. In order to measure the electrical properties, platinum top electrodes with a thickness of 150 nm and a diameter of 100 μm were deposited at room temperature by electron beam evaporation with an *in situ* metal shadow mask.

Results and discussion

GO samples used in our experiments were prepared by the modified Staudemire procedure, and then were reduced by hydrazine hydrate. All active anchor sites were occupied by thionine molecules since the thionine was in large excess to rGO. The rGO–th aqueous solution at a low concentration (*e.g.*, 0.05 mg mL^{-1}) is very stable, and the resultant rGO–th sheets do not precipitate at ambient conditions even after more than one year. The absorption band at ∼600 nm in the UV-vis spectrum (as shown in Fig. 1a and its inset) indicates that rGO was modified successfully by thionine molecules although the band corresponding to the absorbance of thionine is very weak, possibly due to the strong background absorption of rGO. The π–π noncovalent interaction between rGO and thionine is evidenced by the observation of significant fluorescence quenching of the thionine emission in the rGO–th hybrid due to electron transfer from thionine to rGO (as shown in Fig. 1b), which is in good agreement with reported results of graphene modified by other largely π-conjugated dye molecules.[12]
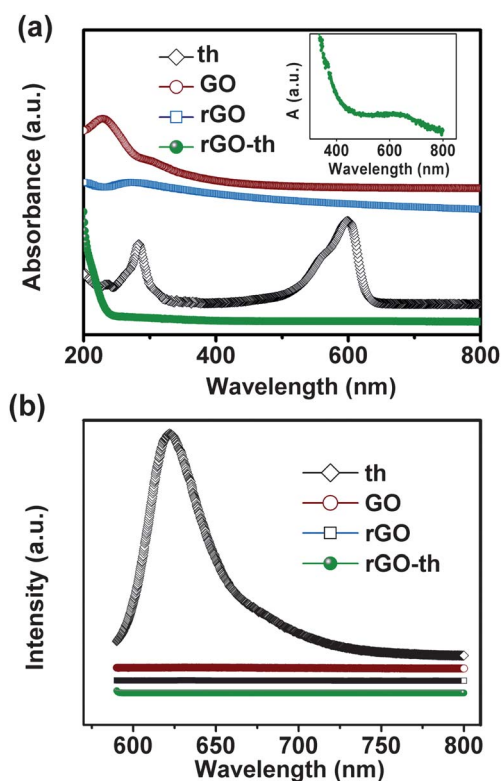
Fig. 1 (a) UV-vis spectra of th, GO, rGO, rGO–th, and the inset is the enlarged spectrum of rGO–th; (b) fluorescence ($\lambda_{ex} = 585$ nm) spectra of th, GO, rGO, rGO–th.

Electrochemical measurements were employed to investigate the bonding and electrically controlled reversible electron transfer between thionine and rGO. The samples were prepared by drop-coating aqueous solutions onto a glassy carbon (GC) electrode. A typical cyclic voltammogram of a thionine-modified GC electrode in phosphate buffer solution shows a couple of small redox peaks (Fig. 2a, curve 2) at −0.219 and −0.206 V. The rGO/GC electrode also presents two redox peaks (Fig. 2a, curve 3), which result from the residual surface-oxygenated species of rGO.[13] In the case of the rGO–th-modified GC electrode, the cyclic voltammogram exhibits well-defined oxidation and reduction peaks at −0.237 and −0.192 V, respectively, with peak currents 30 times larger than that for the th/GC electrode (Fig. 2a, curve 5). The electrochemical measurements clearly demonstrate an electrically controlled reversible electron transfer between rGO and thionine, which leads to much larger oxidation and reduction currents. Furthermore, we investigated the effect of the bonding between rGO and thionine on the reversible electron transfer. For the purpose of comparison, a th/rGO bilayer was drop-coated onto a GC electrode, forming a th/rGO/GC structure. To prepare th/rGO samples, an rGO layer was firstly modified on the GC electrode, and then it was covered with a thin thionine layer by drop-coating with aqueous thionine on the rGO layer. The bonding between rGO and thionine in the th/rGO bilayer should be weaker than that in rGO–th hybrid, considering that the π–π noncovalent interactions occur at the atomic scale in the latter. The cyclic voltammogram of the th/rGO/GC electrode exhibits two redox peaks with oxidation and reduction currents only 8 times larger than those of the th/

GC electrode (Fig. 2a, curve 4), which are almost 4 times lower than those of the rGO–th/GC electrode. Therefore, as shown in Fig. 2b, the electrically controlled reversible electron transfer between thionine and rGO in the rGO–th hybrid is enhanced due to the π–π noncovalent interactions.

The XPS spectra in Fig. 3 demonstrate the elementary composition of GO, rGO and rGO–th. There is a significant increase of carbon content in rGO–th compared to GO, indicating that the rGO–th has been partly deoxygenated. The total C/O atomic ratios of GO and rGO–th are 3.27 and 6.70, respectively. The N 1s and S 2p peaks in XPS spectra of rGO–th clearly indicate that thionine molecules are bonded to rGO sheets. Furthermore, AFM and HRTEM are employed to measure the thickness of the rGO–th nano-hybrid. The single layer graphene nanosheets are almost transparent and very stable under the electron beam (Fig. 4b–d). HRTEM observations give the evidence for the modification of rGO with thionine (Fig. 4e). From the AFM and HRTEM images, it can be seen that the interplanar spacing of the layers is less than 1 nm, which is larger than that (∼0.35 nm) of multi-layer graphene sheets while smaller than that (1–2 nm) of multi-layer GO sheets, indicating a different structure of rGO–th from graphene and GO.

The Pt/rGO–th/Pt memory devices were fabricated and the schematic structure is depicted in Fig. 5a. The resistance of the as-fabricated devices is as high as $\sim7 \times 10^7$ Ω and this pristine device state is defined as the OFF state or high resistance state (HRS). During the I–V measurement, the bottom electrode was grounded. The typical resistance switching process, current–voltage (I–V) characteristics of Pt/rGO–th/Pt devices is shown in Fig. 5b. By increasing the positive voltages imposed on the device, the current increases abruptly at ∼2.5 V (sweep 1), indicating that the device switches from a HRS to a low resistance state (LRS or ON state). The switching from HRS to LRS is called the SET or Write process. A current compliance (1 mA in this work) is usually needed during the SET process to prevent the sample from a permanent breakdown. By sweeping the voltage from 4 to −0.3 V, the device holds on the LRS (sweeps 2 and 3), suggesting nonvolatile memory characteristics. Once the voltage exceeds −0.3 V, the device switches from the LRS to HRS, which is called the RESET or Erase process. The HRS can be retained in the next Read process (sweep 4). The above operations from sweeps 1 to 4 are an entire Write-Read-Erase-Read process. A high ON/OFF ratio of about 5×10^4 is achieved at 0.1 V in this memory device. What should be emphasized is that the reset current (∼0.74 mA) here is lower than the current compliance of 1 mA, which suggests the resistive switching mechanism of Pt/rGO–th/Pt is different from the metal filament mechanism.[6a,6j]

The programming speed, a key criterion for evaluating a memory device, of the Pt/rGO–th/Pt devices was tested by applying pulse stimuli. Fig. 5c illustrates a sequence of Write/Erase cycles stimulated by short pulses, 5 V in height and 5 ns in width for Write and −3 V in height and 5 ns in width for Erase processes, respectively. The measurements are conducted after the as-fabricated device undergoes a few switching cycles, and a small dc voltage of 0.1 V is used to read out the resistance states. From Fig. 5c, it can be seen that the switching process is reproducible from cycle to cycle, confirming the feasibility of switching the present devices by 5 ns pulses. Considering that the
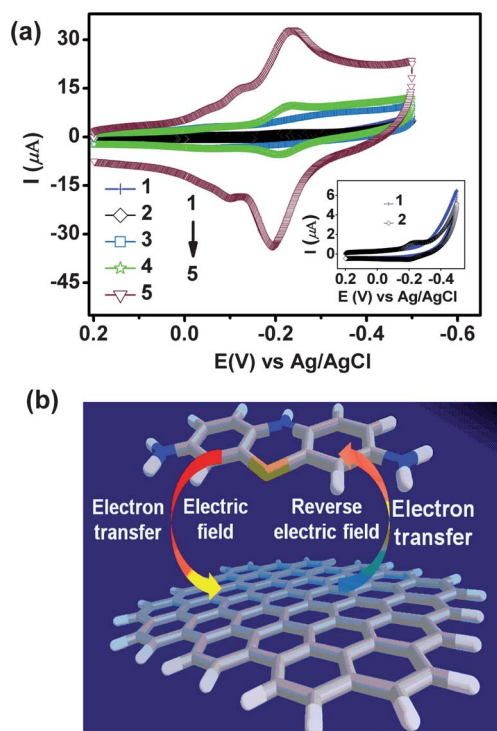
Fig. 2 (a) Cyclic voltammograms of a modified glassy carbon electrode in phosphate buffer solution with: bare electrode (1), thionine (2), rGO (3), th/rGO (4), rGO–th (5) at a scan rate of 100 mV s⁻¹; (b) schematic diagram of bidirectional electron transfer under an electric field.
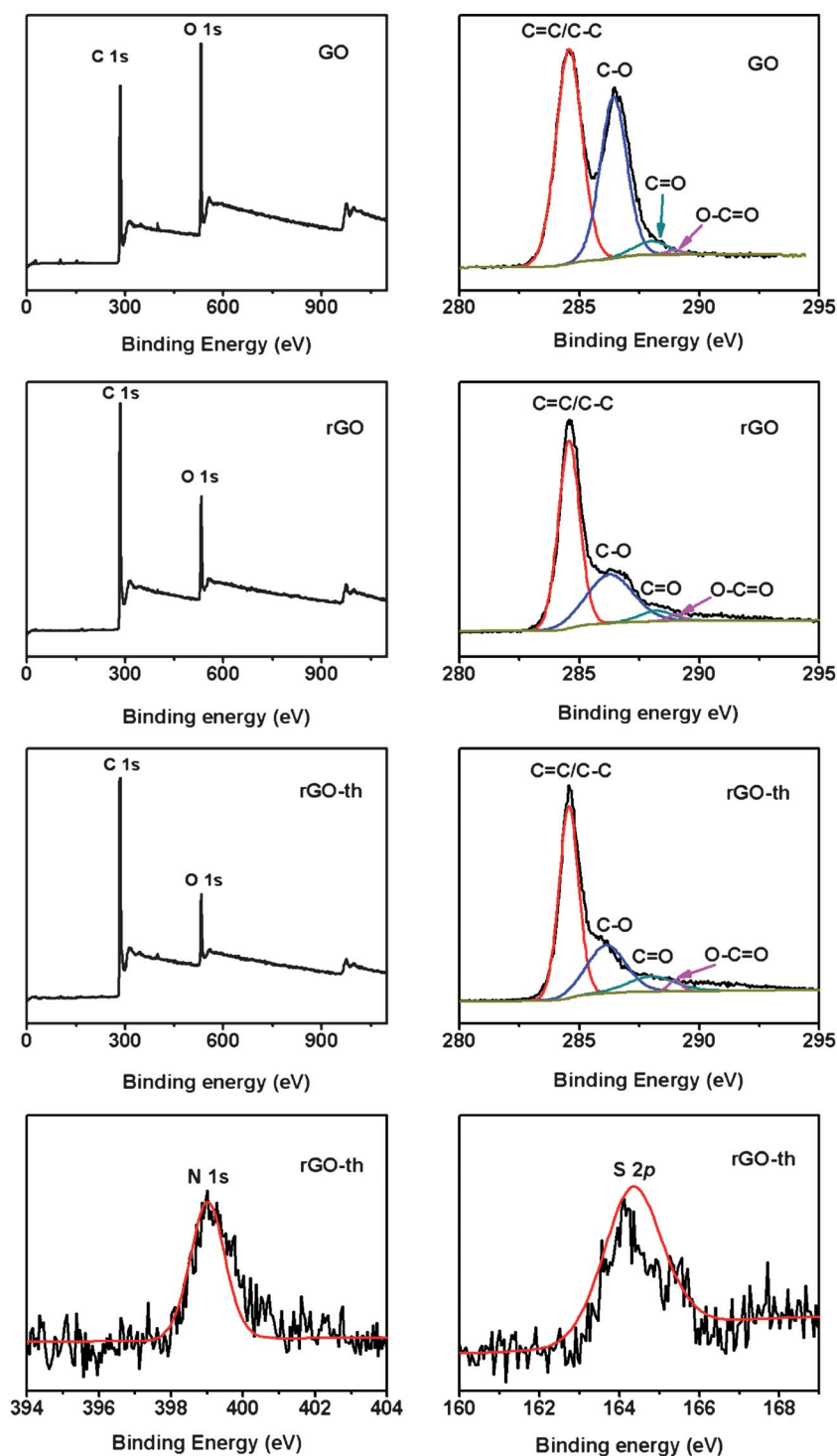
Fig. 3 X-ray photoelectron spectra of GO, rGO and rGO–th.

pulse width of 5 ns nearly approaches the instrument's testing limit, the programming speed of our memory devices is likely to be faster than 5 ns. In fact, the electron transfer speed is expected to break nanosecond and reach picosecond or even femtosecond scale.[14]

In order to clarify the effect of the electron transfer between GO and thionine on the resistive switching, Pt/GO/Pt and Pt/th/Pt were prepared and the resistive switching of pure GO and pure thionine was investigated. Different from devices based on GO with an electrochemically active metal as electrodes, Pt/GO/Pt has a large SET voltage and was ready to break down, which is similar to previously reported results.[15] The Pt/GO/Pt device shows a reset current higher than the current compliance, which is different from Pt/rGO–th/Pt. The unstable resistive switching of Pt/GO/Pt may originate from the irreversible desorption of oxygen-related groups.[6a] On the other hand, as shown in Fig. 6b,
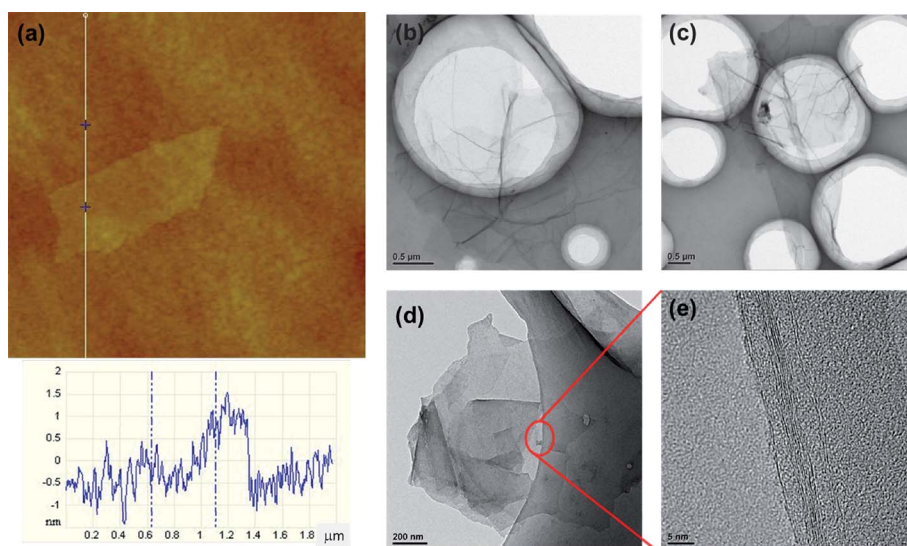
Fig. 4 (a) AFM and (b–e) TEM images of rGO–th.

the Pt/th/Pt showed unstable resistive switching (RS) behavior, which could be ascribed to the fact that thionine is readily oxidated. As a result, we concluded that the electron transferring between the GO and thionine results in stable RS behavior in the Pt/rGO–th/Pt devices.

To exclude the effects of the electrode leading to the RS property, different metal electrodes including inert platinum and electrochemically active copper were used as top electrodes and the RS behavior was characterized. As shown in Fig. 7, both Pt/rGO–th/Cu and Pt/rGO–th/Pt devices exhibit similar bipolar resistive switching, implying that the observed RS behavior is independent of the electrode material, and rather originates from the intrinsic character of the rGO–th film.

In order to investigate the endurance performance of the Pt/rGO–th/Pt memory device, cyclic switching operations were conducted. Fig. 8a illustrates the evolution of resistance of the two well-resolved states over more than 350 cycles. The resistance values are read out at 0.1 V in each dc sweep. Although the resistance of the HRS and LRS scatters to a certain extent, the ON/OFF ratio is more than 10^4 and the resistances did not show degradation after 350 cycles. Fig. 8b illustrates the evolution of SET and RESET voltages of a Pt/rGO–th/Pt memory cell over 350 cycles. When the cell is repeatedly switched between ON and OFF states, the RESET voltage distributes in a range of -0.47 to -1.04 V, while the SET voltage in the range of 1.91–3.93 V. The endurance measurements ensure that the resistance
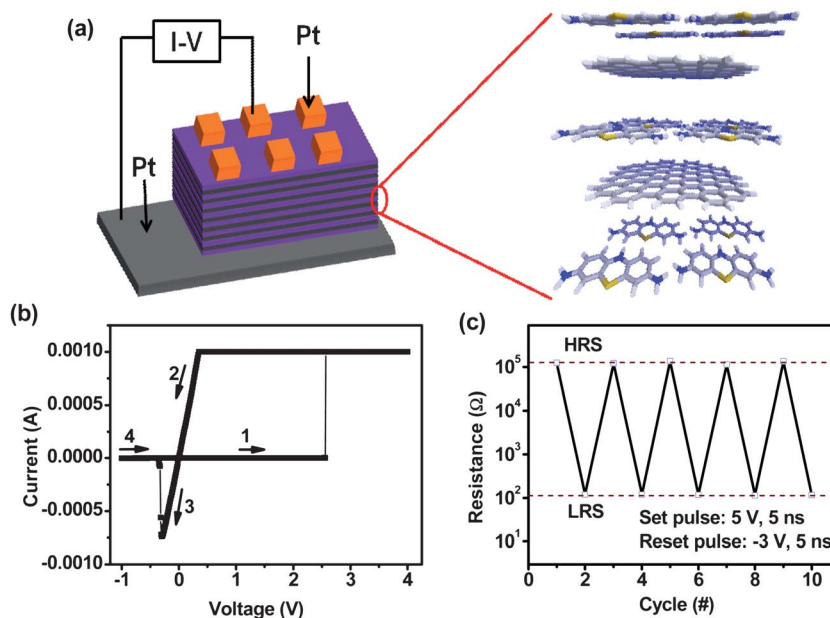
Fig. 5 (a) Schematics of rGO–th based memory device Pt/rGO–th/Pt, (b) *I–V* characteristics of Pt/rGO–th/Pt devices, (c) Write/erase cycles of a Pt/rGO–th/Pt memory device utilizing short pulses of 5 V and 5 ns pulse for writing and -3 V and 5 ns pulse for erasing.

16426 | *J. Mater. Chem.*, 2012, **22**, 16422–16430

This journal is © The Royal Society of Chemistry 2012
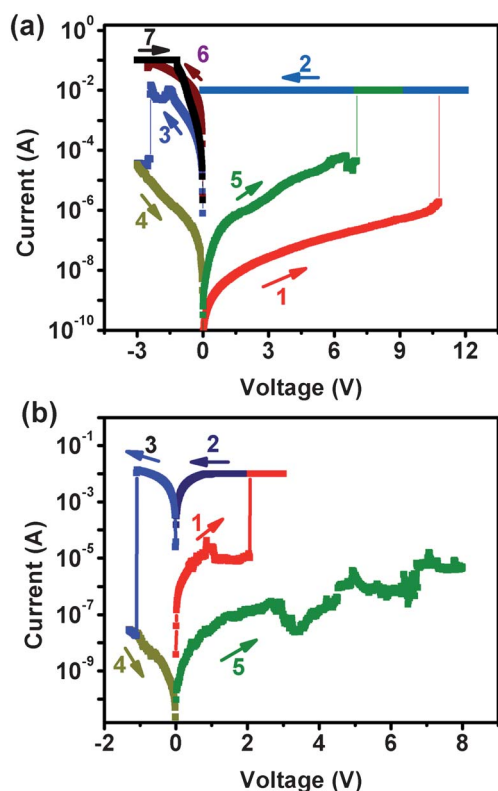
Fig. 6 *I–V* characteristics of (a) Pt/GO/Pt and (b) Pt/th/Pt.
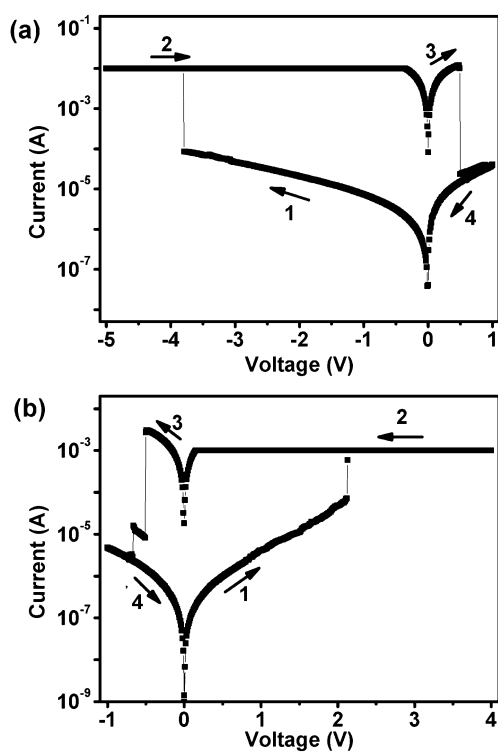
Fig. 7 (a) *I–V* characteristics of the Pt/rGO–th/Pt structure with negative bias in the SET sweep and positive bias in the RESET sweep. (b) *I–V* characteristics of the Pt/rGO–th/Cu structure.
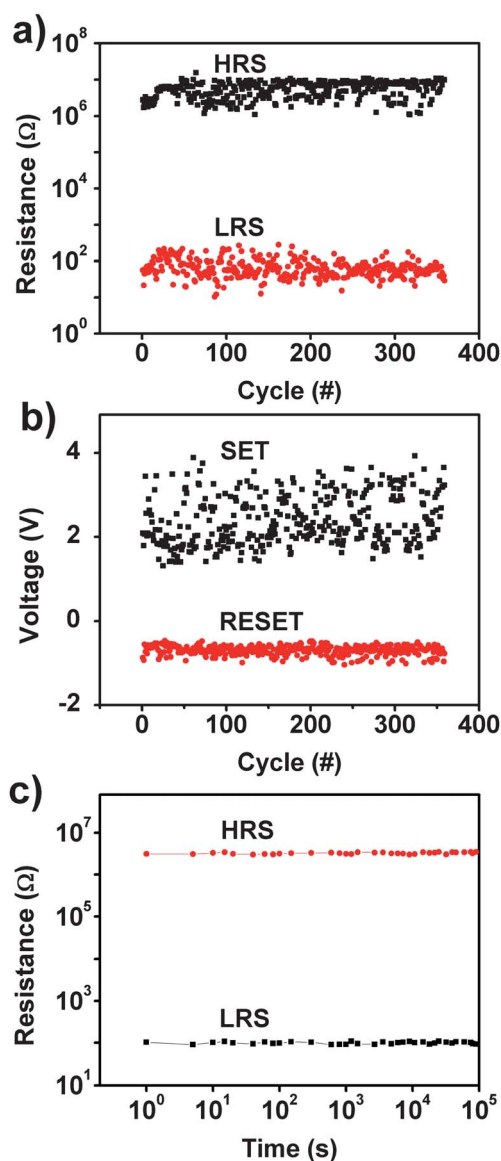
Fig. 8 (a) Endurance performance, (b) distribution of programming voltages (V_{SET} and V_{RESET}), (c) retention of a Pt/rGO–th/Pt device at room temperature.

switching is controllable, reversible, and reproducible. Fig. 8c shows the retention performance of the memory cell at room temperature. The readout is found to be nondestructive. Both the LRS and HRS states can be retained for more than 10^5 s without an external electrical power supply, indicating that the memory device is nonvolatile and stable at room temperature.

A density functional theory (DFT) calculation within the generalized gradient approximation (GGA) of the Perdew–Wang 91 (PW91) form[16] to the exchange–correlation functional was carried out to study the electron transfer between thionine and rGO and the resistive switching mechanism of the Pt/rGO–th/Pt device. For simplicity, well-defined graphene is used instead of poorly defined GO in our model, since the exact structure of GO is difficult to predict. Both graphene and GO could provide a carbon-based network and thus a π-conjugated backbone. The π electrons' transfer behavior along the direction vertical to the

GO plane is induced by an electric field, which is the key to the realization of resistive switching. So GO is modeled as graphene to provide the carbon-based network, and this nature will not change. A supercell model is used. The hydrogen atoms in the redox reaction may be transferred to various oxygen-related groups in rGO and residual water, so it is very difficult to estimate the exact sites where these hydrogen atoms will be transferred for calculation. The exact sites of hydrogen atoms may affect the value of the current vertical to the GO plane but it is not sufficient to cause a change of resistive states. So here we concentrated on the charge transfer behavior between thionine (or leucothionine) and the graphene plane. In the initial state, a sandwich configuration of a leucothionine molecule inserted in between two 4×4 graphene unit cells is considered instead of an actual multi-layer complex. A bilayer model consisting of a thionine molecule absorbed on a 4×4 graphene unit cell (see the black box in Fig. 9a-5) is also applied in some cases. A vacuum space of 40 Å is placed to avoid interaction between the monolayer and its periodic images. The geometry optimization and electronic structures are calculated with the all-electron double numerical atomic orbital plus polarization (DNP) basis set[17] implemented in the DMol[3] package.[18] The convergence criterion of the maximum force on each atom during geometry optimization is 0.01 V Å^{-1}. A $16 \times 16 \times 1$ Monkhorst-Pack[19] k-points grid is used in the first Brillouin zone sampling.

In the as-fabricated device, parts of the dye molecules are at a reduced state (leucothionine). The optimized smallest interatomic distances between leucothionine and the top and bottom graphene of the sandwich structure (Fig. 9a-1) are both 3.20 Å. Since electrons are scattered by the small quantity of unreduced epoxide and hydroxyl groups in the center of GO nanosheets and line-edge roughness carboxyl groups, the initial resistance of the Pt/rGO–th/Pt cell is as high as 7×10^7 Ω and the device is in the OFF state (HRS). According to Mulliken population analysis, in this sandwich structure, 0.067 electrons per supercell are transferred from leucothionine to the graphene sheet under a zero field. Under a vertical electrical field, the thionine molecule is ready to be reversibly reduced or oxidized. The I–V characteristics are independent of the initial direction of $E_\perp$, which is observed in the experiment and verified in our charge transfer calculation. Applying an $E_\perp$ of 0.05 V Å^{-1}, 0.023 additional electrons per supercell are transferred from leucothionine to its lower graphene while no appreciable additional electrons are transferred from the upper graphene to leucothionine (Fig. 9a-2). Changing the direction of $E_\perp$, 0.023 additional electrons per supercell are transferred from leucothionine to its upper graphene while no appreciable additional electrons are transferred from the lower graphene to leucothionine. This electrical-field-induced significant intermolecular charge transfer between leucothionine and one adjacent graphene can be further confirmed
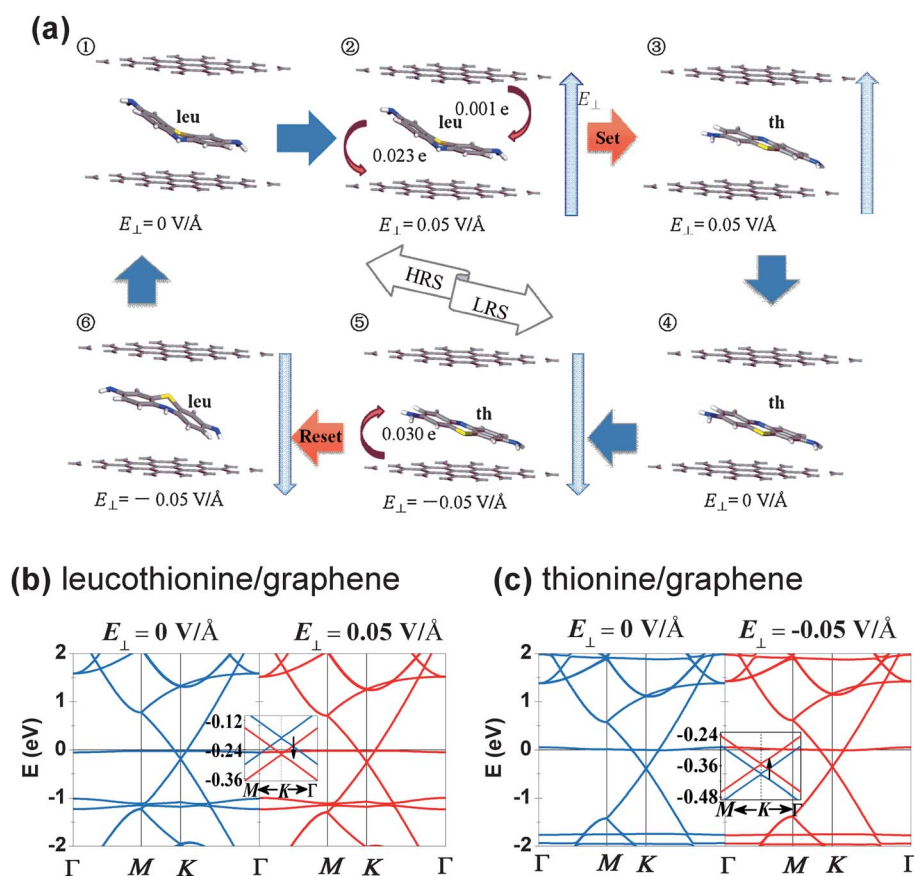
Fig. 9 (a) Geometric model of the rGO–th sandwich and corresponding electron transfer routes (red arrows) under an electric field ($E_\perp$). The blue arrows indicate the direction of the applied $E_\perp$. Key: th = thionine, leu = leucothionine. (b and c) Band structures of the bilayer configuration consisting of graphene and leucothionine (b) and thionine (c) without (left panel) and with (right panel) $E_\perp$ at the GGA/DNP level. The Fermi level is set to zero. Insets: Band structures near the Dirac point. The positive direction of $E_\perp$ is upward.

by the band structure. Because the charge transfer only takes place between leucothionine and one graphene sheet, we focus on the band structure of a bilayer consisting of leucothionine and the charge-transfer-related graphene. Fig. 9b shows the band structure of a leucothionine/graphene bilayer under $E_\perp = 0$ and 0.05 V $\mathring{A}^{-1}$, respectively. The horizontal line near the Fermi level (E_f) is from the dye molecule and crosses the π^* band of graphene under zero field. The Dirac point is 0.20 eV lower than E_f under zero field and becomes 0.26 eV lower than E_f under $E_\perp = 0.05$ V $\mathring{A}^{-1}$, as a result of electron acceptance from the HOMO level of leucothionine.

Consequently, leucothionine is oxidized to thionine. Different from the V-shape of leucothionine, thionine is a quasi-planar molecule, which augments the π–π interactions over the whole nanocomposite. The transferred electrons are delocalized effectively in the giant π-conjugation system and further reduce the GO. Electrons can transport with less scattering, leading to a substantially enhanced conductivity of the complex. At the threshold voltage, we guess some thionine molecules and further reduced GO will connect to form a conductive path between two electrodes for the charge to transport with little hindrance. Thus the device is set to the ON state (LRS) as shown in Fig. 9a-3.

A further comparison of the transport properties between the leucothionine/graphene and thionine/graphene systems was performed and has proven our assumption. A Pt atom is placed 3 $\mathring{A}$ above the dye molecule in the dye/graphene bilayer structures. When $E_\perp = 0.05$ V $\mathring{A}^{-1}$, the Pt atom in both systems loses about 0.01 electrons. In the leucothionine/graphene system, charge communication only exists between the Pt atom and leucothionine while the graphene does not participate. However, in the thionine/graphene system, the graphene sheet accepts 0.13 electrons per supercell from the Pt atom and thionine. It appears that the thionine is a charge transmission medium in the rGO–th multi-layer complex and the Pt electrodes act as an electron reservoir that provides sufficient electrons for transmission. Thereby, the electrons transmit with little hindrance through the conductive path formed by thionine and graphene, and a stable electric current arises leading the device into the ON state.

When the positive $E_\perp$ is reduced gradually, the low resistive state remains as illustrated in sweep 2 of Fig. 5b and so the thionine is not reduced into leucothionine after the $E_\perp$ is removed. We suppose this process (Fig. 9a-3 to a-4) to be irreversible and the charge populations of thionine and graphene are basically unchanged. When a reverse small $E_\perp$ is applied, the device is still in the LRS at first (sweep 3 in Fig. 5b). However, the resistance increases suddenly when the reverse $E_\perp$ reaches a critical value. As a cation, thionine is closer to its lower graphene under the influence of an electrical force. Thus, the rGO–th multi-layer complex is turned into a state that is not symmetric from up to down, and the thionine/graphene bilayer model appears more proper than the sandwich one for analysis. Applying a reverse $E_\perp$ of -0.05 V $\mathring{A}^{-1}$, 0.03 additional electrons per supercell are transferred from the graphene to thionine, and the Dirac point of graphene moves upward by 0.04 eV as shown in Fig. 9c. When the thionine is reduced (into leucothionine), the rGO–th multi-layer complex will restore to the initial low conductive oxide form and the device is reset to the OFF state (Fig. 9a-5 to a-6).

Conclusions

Electrically controlled bidirectional electron transfer between reduced graphene oxide noncovalently functionalized by thionine in the form of a homogeneous solution and films was demonstrated experimentally and theoretically. The sandwiched devices based on rGO–th functionalized noncovalently by thionine molecules show nonvolatile resistive switching behavior with an ON/OFF ratio of more than 10^4, fast switching speed of <5 ns, long retention time of over 10^5 s and good endurance. These results provide a new strategy for controlling the electronic properties of graphene for high performance memory device applications.

Acknowledgements

References

1 K. S. Novoselov, A. K. Geim, S. V. Morozov, D. Jiang, Y. Zhang, S. V. Dubonos, I. V. Grigorieva and A. A. Firsov, *Science*, 2004, **306**, 666.

2 (a) A. K. Geim and K. S. Novoselov, *Nat. Mater.*, 2007, **6**, 183; (b) J. C. Meyer, A. K. Geim, M. I. Katsnelson, K. S. Novoselov, T. J. Booth and S. Roth, *Nature*, 2007, **446**, 60; (c) J. Wu, W. Pisula and K. Müllen, *Chem. Rev.*, 2007, **107**, 718.

3 (a) H. Wang, Y. Wu, C. Cong, J. Shang and T. Yu, *ACS Nano*, 2010, **4**, 7221; (b) M. J. Allen, V. C. Tung, L. Gomez, Z. Xu, L. M. Chen, K. S. Nelson, C. W. Zhou, R. B. Kaner and Y. Yang, *Adv. Mater.*, 2009, **21**, 2098.

4 (a) N. Yang, J. Zhai, D. Wang, Y. Chen and L. Jiang, *ACS Nano*, 2010, **4**, 887; (b) V. C. Tung, L. M. Chen, M. J. Allen, J. K. Wassei, K. Nelson, R. B. Kaner and Y. Yang, *Nano Lett.*, 2009, **9**, 1949.

5 Z.-S. Wu, W. Ren, L. Xu, F. Li and H.-M. Cheng, *ACS Nano*, 2011, **5**, 5463.

6 (a) C. L. He, F. Zhuge, X. F. Zhou, M. Li, G. C. Zhou, Y. W. Liu, J. Z. Wang, B. Chen, W. J. Su, Z. P. Liu, Y. H. Wu, P. Cui and R.-W. Li, *Appl. Phys. Lett.*, 2009, **95**, 232101; (b) G. Liu, X. Zhuang, Y. Chen, B. Zhang, J. Zhu, C.-X. Zhu, K.-G. Neoh and E.-T. Kang, *Appl. Phys. Lett.*, 2009, **95**, 253301; (c) H. Y. Jeong, J. Y. Kim, J. W. Kim, J. O. Hwang, J.-E. Kim, J. Y. Lee, T. H. Yoon, B. J. Cho, S. O. Kim, R. S. Ruoff and S.-Y. Choi, *Nano Lett.*, 2010, **10**, 4381; (d) J. Liu, Z. Yin, X. Cao, F. Zhao, A. Lin, L. Xie, Q. Fan, F. Boey, H. Zhang and W. Huang, *ACS Nano*, 2010, **4**, 3987; (e) X.-D. Zhuang, Y. Chen, G. Liu, P.-P. Li, C.-X. Zhu, E.-T. Kang, K.-G. Noeh, B. Zhang, J.-H. Zhu and Y.-X. Li, *Adv. Mater.*, 2010, **22**, 1731; (f) P. Cui, S. Seo, J. Lee, L. Wang, E. Lee, M. Min and H. Lee, *ACS Nano*, 2011, **5**, 6826; (g) S. K. Hong, J. E. Kim, S. E. Kim and B. J. Cho, *J. Appl. Phys.*, 2011, **110**, 044506; (h) S. Wang, K. K. Manga, M. Zhao, Q. Bao and K. P. Loh, *Small*, 2011, **7**, 2372; (i) B. Zhang, Y. Chen, L. Xu, L. Zeng, Y. He, E.-T. Kang and J. Zhang, *J. Polym. Sci., Part A: Polym. Chem.*, 2011, **49**, 2043; (j) F. Zhuge, B. Hu, C. He, X. Zhou, Z. Liu and R.-W. Li, *Carbon*, 2011, **49**, 3796; (k) A.-D. Yu, C. L. Liu and W.-C. Chen, *Chem. Commun.*, 2012, **48**, 383.

7 (a) R. A. Nistor, D. M. Newns and G. J. Martyna, *ACS Nano*, 2011, **5**, 3096–3103; (b) Z. Chen, S. Berciaud, C. Nuckolls, T. F. Heinz and L. E. Brus, *ACS Nano*, 2010, **4**, 2964–2968; (c) N. V. Kozhemyakina, J. M. Englert, G. Yang, E. Spiecker, C. D. Schmidt, F. Hauke and

A. Hirsch, *Adv. Mater.*, 2010, **22**, 5483; (*d*) J. M. Englert, J. Röhrl, C. D. Schmidt, R. Graupner, M. Hundhausen, F. Hauke and A. Hirsch, *Adv. Mater.*, 2009, **21**, 4265; (*e*) C. Gómez-Navarro, R. T. Weitz, A. M. Bittner, M. Scolari, A. Mews, M. Burghard and K. Kern, *Nano Lett.*, 2007, **7**, 3499; (*f*) O. V. Yazyev and S. G. Louie, *Nat. Mater.*, 2010, **9**, 806; (*g*) P. Avouris, Z. Chen and V. Perebeinos, *Nat. Nanotechnol.*, 2007, **2**, 605; (*h*) T. Ohta, A. Bostwick, T. Seyller, K. Horn and E. Rotenberg, *Science*, 2006, **313**, 951; (*i*) R. M. Westervelt, *Science*, 2008, **320**, 324.

8 (*a*) C. Backes, F. Hauke and A. Hirsch, *Adv. Mater.*, 2011, **23**, 2588; (*b*) L. Wang, K.-Y. Pu, J. Li, X. Qi, H. Li, H. Zhang, C. Fan and B. Liu, *Adv. Mater.*, 2011, **23**, 4386; (*c*) Y. Xu, Z. Liu, X. Zhang, Y. Wang, J. Tian, Y. Huang, Y. Ma, X. hang and Y. S. Chen, *Adv. Mater.*, 2009, **21**, 1275; (*d*) J. Malig, N. Jux, D. Kiessling, J.-J. Cid, P. Vázquez, T. Torres and D. M. Guldi, *Angew. Chem., Int. Ed.*, 2011, **50**, 3561.

9 (*a*) J. A. Mann, J. Rodriguez-Lopez, H. D. Abruna and W. R. Dichtel, *J. Am. Chem. Soc.*, 2011, **133**, 17614; (*b*) W. Tu, J. Lei, S. Zhang and H. Ju, *Chem.–Eur. J.*, 2010, **16**, 10771; (*c*) Z. Sun, C. L. Pint, D. C. Marcano, C. Zhang, J. Yao, G. Ruan, Z. Yan, Y. Zhu, R. H. Hauge and J. M. Tour, *Nat. Commun.*, 2011, **2**, 559.

10 (*a*) J. Clavilier, V. Svetličić and V. J. Žutić, *J. Electroanal. Chem.*, 1995, **386**, 157; (*b*) V. E. Nicotra, M. F. Mora, R. A. Iglesias and A. M. Baruzzi, *DyesPigm.*, 2008, **76**, 315; (*c*) C. Chen, W. Zhai, D. Lu, H. hang and Z. G. Zheng, *Mater. Res. Bull.*, 2011, **46**, 583.

11 H.-B. Zhang, W.-G. Zheng, Q. Yan, Y. Yang, J.-W. Wang, Z.-H. Lu, G.-Y. Ji and Z.-Z. Yu, *Polymer*, 2010, **51**, 1191.

12 (*a*) Y. Xu, H. Bai, G. Lu, C. Li and G. Shi, *J. Am. Chem. Soc.*, 2008, **130**, 5856; (*b*) H.-C. Cheng, R.-J. Shiue, C.-C. Tsai, W.-H. Wang and Y.-T. Chen, *ACS Nano*, 2011, **5**, 2051; (*c*) K. P. Loh, Q. Bao, P. K. Ang and J. Yang, *J. Mater. Chem.*, 2010, **20**, 2277; (*d*) K. P. Loh, Q. Bao, G. Eda and M. Chhowalla, *Nat. Chem.*, 2010, **2**, 1015.

13 (*a*) M. Zhou, Y. Zhai and S. Dong, *Anal. Chem.*, 2009, **81**, 5603; (*b*) M. Zhou, Y. Wang, Y. Zhai, J. Zhai, W. Ren, F. Wang and S. Dong, *Chem.–Eur. J.*, 2009, **15**, 6116.

14 (*a*) G. M. A. Rahman, D. M. Guldi, S. Campidelli and M. Prato, *J. Mater. Chem.*, 2006, **16**, 62; (*b*) C. Roquelet, D. Garrot, J. S. Lauret, C. Voisin, V. Alain-Rizzo, P. Roussignol, J. A. Delaire and E. Deleporte, *Appl. Phys. Lett.*, 2010, **97**, 141918.

15 (*a*) O. Ö. Ekiz, M. Urel, H. Güner, A. K. Mizrak and A. Däna, *ACS Nano*, 2011, **5**, 2475; (*b*) J. M. Mativetsky, E. Treossi, E. Orgiu, M. Melucci, G. P. Veronese, P. Samorì and V. Palermo, *J. Am. Chem. Soc.*, 2010, **132**, 14130.

16 J. P. Perdew, *Phys. B*, 1991, **172**, 1.

17 B. J. Delley, *Chem. Phys.*, 1990, **92**, 508.

18 B. J. Delley, *Chem. Phys.*, 2000, **113**, 7756.

19 H. J. Monkhorst and J. D. Pack, *Phys. Rev. B: Solid State*, 1976, **13**, 5188.